# Analytical modelling of near-source pulse-like seismic demand for multi-linear backbone oscillators

Georgios Baltzopoulos[1],[*],[†], Dimitrios Vamvatsikos[2] and Iunio Iervolino[1]

[1]*Dipartimento di Strutture per l'Ingegneria e l'Architettura, Università degli Studi di Napoli Federico II, Naples, Italy*
[2]*School of Civil Engineering, National Technical University of Athens, Athens, Greece*

## SUMMARY

Nonlinear static procedures, which relate the seismic demand of a structure to that of an equivalent single-degree-of-freedom oscillator, are well-established tools in the performance-based earthquake engineering paradigm. Initially, such procedures made recourse to inelastic spectra derived for simple elastic–plastic bilinear oscillators, but the request for demand estimates that delve deeper into the inelastic range, motivated investigating the seismic demand of oscillators with more complex backbone curves. Meanwhile, near-source (NS) pulse-like ground motions have been receiving increased attention, because they can induce a distinctive type of inelastic demand. Pulse-like NS ground motions are usually the result of rupture directivity, where seismic waves generated at different points along the rupture front arrive at a site at the same time, leading to a double-sided velocity pulse, which delivers most of the seismic energy. Recent research has led to a methodology for incorporating this NS effect in the implementation of nonlinear static procedures. Both of the previously mentioned lines of research motivate the present study on the ductility demands imposed by pulse-like NS ground motions on oscillators that feature pinching hysteretic behaviour with trilinear backbone curves. Incremental dynamic analysis is used considering 130 pulse-like-identified ground motions. Median, 16% and 84% fractile incremental dynamic analysis curves are calculated and fitted by an analytical model. Least-squares estimates are obtained for the model parameters, which importantly include pulse period $T_p$. The resulting equations effectively constitute an $R - \mu - T - T_p$ relation for pulse-like NS motions. Potential applications of this result towards estimation of NS seismic demand are also briefly discussed. Copyright © 2016 John Wiley & Sons, Ltd.

## 1. INTRODUCTION

One of the key issues in performance-based earthquake engineering (e.g. [1]) is the assessment of seismic demand for structures expected to respond inelastically to future earthquakes attaining a certain intensity. Near-source (NS) seismic input merits special attention, because NS ground motions often contain prominent wave pulses. In fact, the engineering relevance of NS pulse-like ground motions has been on the rise during the past decades, because it has been recognized that such ground motions can induce a distinctive type of inelastic demand and can be more damaging than motions not displaying similar impulsive features. Perhaps the most important, although not unique, phenomenon that can cause NS strong ground motion to exhibit such pulse-like characteristics is rupture forward directivity (FD). Directivity can occur because during fault rupture the propagation velocity of shear dislocation along the fault will typically be near shear wave

---

*Correspondence to: Georgios Baltzopoulos, Dipartimento di Strutture per l'Ingegneria e l'Architettura, Università degli Studi di Napoli Federico II, via Claudio 21, 80125, Naples, Italy;
[†]E-mail: georgios.baltzopoulos@unina.it

velocity. As a consequence, there is a probability for shear wave fronts emitted from different points along the fault to arrive almost simultaneously at sites aligned along the direction of rupture propagation. This phenomenon can give rise to a constructive wave interference effect, which is typically observable in the velocity recording as a single double-sided, early-arriving pulse that contains most of the seismic energy [2, 3]. One such example of pulse-like ground motion registered during the 2009 L'Aquila earthquake (Italy) is given in Figure 1, where the impulsive waveform extracted from the velocity time-history by means of the algorithm proposed by Baker [4] and the associated pulse period $T_p$ are shown, along with the corresponding score assigned by said algorithm to various horizontal orientations of the record.

On the other hand, procedures relating the structural seismic demand to that of an equivalent single-degree-of-freedom (SDOF) oscillator, collectively known as nonlinear static procedures [5, 6], have gradually found their way into performance-based earthquake engineering and modern codes for seismic design and assessment. At first, static nonlinear procedures based on inelastic spectra (e.g. [7]) employed spectra obtained from simple elastic-perfectly-plastic or bilinear oscillators. The adaptation of one such procedure for applicability in NS conditions has been already suggested [8]. However, the request for demand estimates that involve larger inelastic deformations and arrive at quantifying collapse capacity (definition to follow) led researchers to also investigate the seismic demand of oscillators with more complex backbone curves such as the trilinear one in Figure 2.

For the complete analytical description of this backbone curve, three parameters are required. First is the slope of a hardening (or perfectly plastic) branch, $\alpha_h$, that simulates post-yield ductility. Second and third are the 'capping point' ductility $\mu_c$ and (negative) slope $\alpha_c$ that define the softening branch. The latter intersects the zero-strength axis at ductility $\mu_{end}$ given by Eqn 1.

$$\mu_{end} = \mu_c + (1 + \mu_c \cdot \alpha_h - \alpha_h)/|\alpha_c| \qquad (1)$$

The presence of such a softening (negative stiffness) branch is typical of the behaviour of most structures, either brittle or ductile, that reach a maximum strength and then exhibit in-cycle degradation that in turn leads to strength loss. The phenomena that actually lead to negative stiffness in a real structure can include $P$-$\Delta$ effects and material strength degradation (often both). Negative stiffness is thus encountered on the static pushover curves of different types of structures, such as braced steel frames, moment-resisting steel frames ([9]), concrete frames ([10]) and any type of structure that exhibits sensitivity to second-order effects ([11]). In general, only systems susceptible
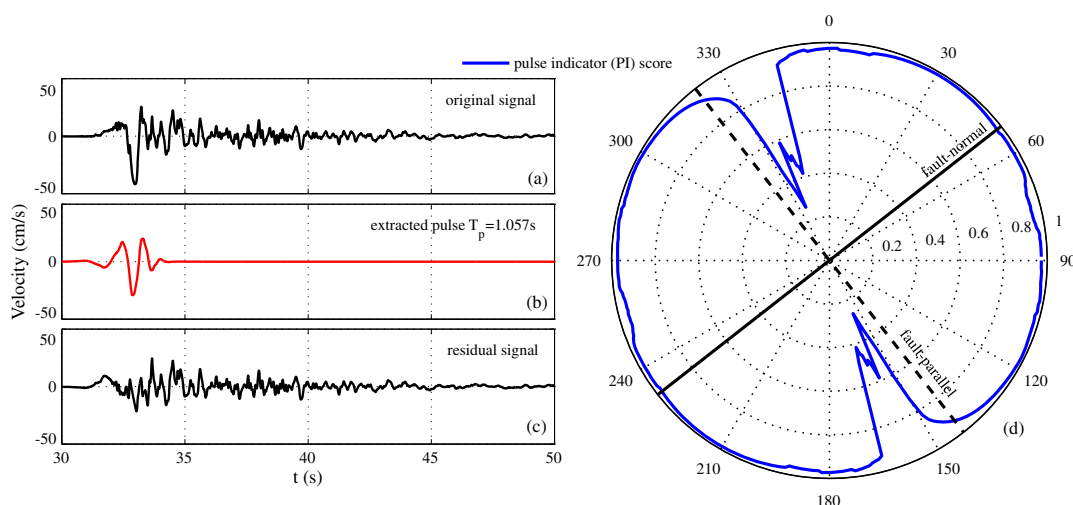


Figure 1. (a) Original velocity time-history of the Valle Aterno–Centro Valle recording (fault-normal component) from the 2009 M6.3 L'Aquila earthquake (Italy), (b) velocity pulse with pulse period $T_p$ extracted by the methodology in [4], (c) residual velocity signal after extraction of the aforementioned pulse, and (d) polar plot of pulse indicator score per azimuth for all horizontal orientations of the same ground motion.
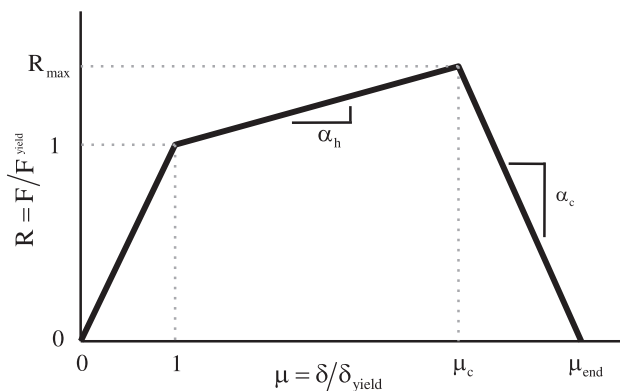
Figure 2. Representation of trilinear backbone curve in normalized coordinates (ductility $\mu$ in the abscissa and reduction factor $R$ in the ordinate) and defining parameters: post-yield hardening slope $\alpha_h$, softening branch negative slope $\alpha_c$, and capping ductility $\mu_c$, which separates the hardening and softening branches.

to brittle failures that abruptly lead to global collapse may exhibit pushover curves ending without a finite-slope negative stiffness segment.

This study employs incremental dynamic analysis (IDA; [12]) in order to investigate the seismic demand of tri-linear backbone oscillators, when subjected to NS-FD ground motions. The ultimate goal is that of developing an analytical model for median NS pulse-like demand and the associated dispersion. IDA can be a computationally intensive procedure. This fact motivated Vamvatsikos and Cornell to develop a software tool, which provides a shortcut, at the cost of introducing some approximation in the process [13]. Having observed that summary IDA curves of SDOF systems with multi-linear backbone curves exhibit a consistent behaviour in correspondence with each segment of the backbone (elastic, post-yield hardening, and post-cap softening segments), they used IDA to investigate the response of a large population of oscillators with varying backbone parameters. Having thus mapped the behaviour of many backbone shapes against a suite of ordinary ground motions, which are unlikely to have been affected by directivity or soft soil, they proposed a tool, aptly named SPO2IDA, capable or reproducing the IDA curves of these SDOF systems without having to run any analysis. Essentially, SPO2IDA is nothing less than a complex $R - \mu - T$ relation applicable to ordinary ground motions [14]. The objective of this study is to adapt the methodology of [13] to the NS case and employ IDA on trilinear backbone SDOF systems using a set of one-hundred and thirty pulse-like ground motions, in order to develop the equivalent of an $R - \mu - T - T_p$ relation for NS-FD ground motions.

The remainder of this article is structured as follows: after a brief note on the ground motion suite employed, the methodology is laid out in detail along with the various considerations that contributed towards the formulation of the analytical model. This is followed by a description of the parameter-fitting procedure and techniques that were employed for the development of the principal analytical components of the model. Finally, some key observations on NS pulse-like response stemming from the proposed equations are made and the applicability of the model is briefly discussed.

## 2. METHODOLOGY

### 2.1. Record set of NS pulse-like ground motions and definition of pulse period

The present study employs a dataset of one-hundred and thirty pulse-like NS ground motions, whose impulsive nature is believed to be related to rupture directivity. The methodologies for pulse identification adopted while assembling this dataset were those suggested in [4] and [15]. The NS-FD ground motion dataset employed in [16] served as a starting point and was subsequently enriched by records from more recent seismic events, such as the Parkfield 2004 (California) event, the Darfield 2010 and Christchurch 2011 (New Zealand) events, and the South Napa 2014 (California)

event. A more detailed account of the considerations that went into the compilation of this NS pulse-like ground motion dataset can be found in [17] along with a complete list of the records and relevant metadata (Chapter 4 and Appendix B of [17]).

Given that the objective of the present study is, ultimately, to characterize NS structural response by means of an analytical model that includes pulse duration $T_p$, it may be worthwhile to briefly discuss the definition and identification of $T_p$. Both pulse identification algorithms mentioned previously employ the same definition of pulse period, which is the pseudo-period of the highest-coefficient wavelet returned by a wavelet transform of the velocity signal. This definition has been found to be efficient, but it is far from unique in the literature (e.g. [18, 19]). Furthermore, both algorithms are known to be occasionally triggered by impulsive waveforms attributed to soft-soil site effects or other causes unrelated to FD.

From the inelastic structural response point of view, one has to take into consideration the fact that velocity pulses significantly deviating from the characteristic double-sided, early-arriving waveform associated with directivity, may not exhibit the same type of correlation between displacement demand and pulse period as FD-related pulses do (e.g. [20]). For this reason, in this work, some efforts were made to discern those velocity pulses most likely to have been the result of directivity for eventual inclusion in this investigation. In fact, Shahi and Baker report their opinion on whether or not the impulsive characteristics of the ground motions analyzed in [15] are because of directivity; their assessment was also taken into account. The least-squares linear regression line of $\ln T_p$ against magnitude of the causal event for this dataset, shown in Figure 3(a), is not far off those reported by other researchers (e.g. [18]).

Finally, as already mentioned, more than one definitions of $T_p$ appear in the literature. For example, [19] employed the period which exhibits the maximum spectral pseudo-velocity (previously termed the predominant period $T_g$ in [21]) to characterize inelastic spectra of NS ground motions. One advantage of the wavelet-based definition of pulse period is that it is not sensitive to competing peaks of local maxima on the pseudo-velocity spectrum (refer for example to [4]). However, the two definitions do produce strongly correlated pulse duration estimates. This can be seen in Figure 3(b), from which it also becomes obvious that $T_g$ displays a consistent trend of corresponding to a duration around 70% of $T_p$. This leads to the conclusion that while no definition of pulse period can be said to be demonstrably superior to all others, some care must be exercised when combining pulse duration information from NS hazard ([22, 23]) with inelastic spectra referring to specific $T/T_p$ ratios (e.g. as in [16, 19]) in order to ascertain that the two are compatible.

## 2.2. Incremental dynamic analysis for SDOF systems using pulse-like NS records

Incremental dynamic analysis is a powerful semi-empirical method for the probabilistic estimation of seismic structural demand and capacity. This well-established procedure, typically entails a non-linear numerical model of the structure that is subjected to a suite of ground motion records, all scaled at a common seismic intensity measure (IM) level. This IM level is gradually increased by applying scaling to all the records, in order to reveal the entire range of post-yield response of the structure, conditional to several IM values, up to global dynamic instability and eventual collapse. During
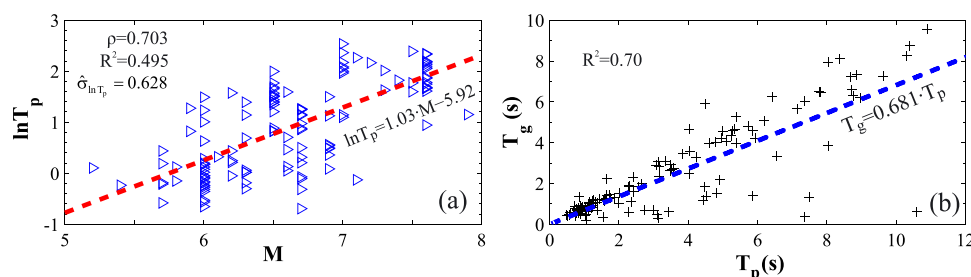


Figure 3. (a) Linear regression of log-pulse period against magnitude and (b) zero-intercept linear regression of pulse period ($T_p$) against period of maximum spectral pseudo-velocity (or predominant period $T_g$). Correlation coefficient ($\rho$), coefficient of determination ($R^2$) and estimator of the standard deviation ($\hat{\sigma}_{\ln T_p}$) are also reported

IDA, structural response to each single record is represented by plotting two scalars against each other: an IM characterizing the various scaled incarnations of the record and an engineering demand parameter (EDP) representing the amplitude of response, resulting in a single-record IDA curve. Once a set of IDA curves has been collected, representing the entire suite of ground motions, it is an efficient practice to summarize the curves into sample statistics; for example medians, 16% and 84% fractiles [24].

The present study entails performing IDA for a large population of SDOF systems, characterized by various bilinear or trilinear backbones. As already indicated, pulse period $T_p$ is considered a key explanatory variable, by virtue of its demonstrable value as a predictor for the inelastic response for this type of ground motion [25, 26]. In fact, pulse period is included as the denominator of the normalized period ratio $T/T_p$, in a manner analogous to [16, 19] (the merit of this decision will see extensive discussion in the following).

Consequently, the computation of IDA curves for the purposes of this work is performed for given values of the $T/T_p$ ratio. Because each record in the suite of NS pulse-like ground motions considered is associated with a different pulse period, this effectively means that each individual IDA curve will correspond to an SDOF oscillator with different period of natural vibration, determined by the requisite of maintaining a constant $T/T_p$ ratio within that particular IDA set. This leads to the IM of choice for these IDAs being the strength reduction factor R, defined as per Eqn 2.

$$R = S_a\left(T_i = \kappa \cdot T_{p,i}, \xi = 5\%\right) / S_a^{yield}(T_i, 5\%), \kappa = T/T_p \in [0.10, 2.00] \qquad (2)$$

On the other hand, EDP of choice for the SDOF systems is ductility $\mu = \delta_{max}/\delta_{yield}$ (defined as the ratio of maximum displacement to displacement at yield).

Therefore, these SDOF IDA curves obtained by scaling a suite of impulsive records (which shall be occasionally referred to as pulse-IDAs for brevity in the remainder of this work) will result in summary fractile curves that collect the responses of diverse oscillators plotted in dimensionless $\{\mu, R\}$ coordinates. An example of such pulse-IDAs can be seen in Figure 4, where the $\{\mu, R\}$ coordinates also permit plotting the curves superimposed against the backbone of the corresponding oscillator. Strictly speaking, there is a subtle difference in the definition of strength reduction factor and ductility used for the representation of the backbone and those used to plot the IDAs. In the case of a monotonic loading backbone curve (e.g. Figure 2), reduction factor and ductility are defined using the instantaneous values of force and displacement on the numerator: $R = F/F_{yield}$ and $\mu = \delta/\delta_{yield}$. On the other hand, in the case of IDA curves, the numerator becomes the maximum absolute value of force or displacement recorded over
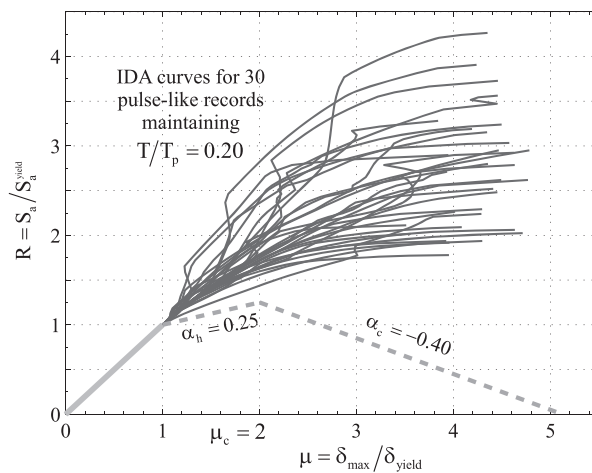


Figure 4. Thirty individual IDA curves of trilinear-backbone SDOF oscillators subjected to pulse-like records. Each curve corresponds to a distinct SDOF system with different vibration period, chosen in order to maintain a constant $T/T_p$ ratio for all pulse-IDAs. The IDA curves are plotted over the oscillators' (common) backbone curve, which is only possible in normalized, dimensionless coordinates (ductility $\mu$—reduction factor R).

the entire time-history of response to a scaled record: $R = F_{max}/F_{yield} = S_a/S_a^{yield}$ and $\mu = \delta_{max}/\delta_{yield}$. However, for the sake of brevity, whenever backbones and IDAs are plotted together (e.g. Figure 4) and hence both definitions apply, only the definitions corresponding to the IDA will be reported on the graph axes.

One final comment to be made about this type of pulse IDAs concerns the actual scaling of the impulsive ground motions. Although scaling is conceptually intrinsic to IDA, some ground motion classification algorithms ([4, 15]) propose maximum ground velocity thresholds, which a record should surpass in order to be identified as pulse-like. This implies that a given pulse-like record, when scaled downwards with respect to its registered amplitude, could cease to satisfy such a classification criterion. However, any evaluation of pulse identification procedures and their implications is certainly beyond the scope of the present work.

### 2.3. Hysteretic rule

For the present study, a peak-oriented, moderately pinching hysteresis rule developed by Ibarra and Krawinkler [27] was adopted for all SDOF systems subjected to IDA. No cyclic strength degradation has been included; eventual loss of strength only occurs when the response crosses capping ductility $\mu_c$ into the softening (negative-stiffness) branch (Figure 2). One of the reasons behind this choice is that when oscillators featuring a descending branch are concerned, it has been established that kinematic hardening hysteresis is not entirely representative of how actual structures have been observed to behave during experiments [28]. Furthermore, the issue of strength degradation is considered to be of secondary importance in this case. Strength degradation only tends to supersede the shape of the backbone in importance when severe degradation is encountered in low-period structures. However, given the range of pulse-periods associated with the NS-FD record suite employed in this study (refer for example in Figure 3 or [17]), the model is more oriented towards moderate to long period structures (refer to next paragraph for the treatment of low period oscillators) and cyclic degradation is not included in the hysteretic rule used in the analyses.

### 2.4. Analytical model for NS pulse-like seismic demand

*2.4.1. Median and scatter of pulse-like seismic demand.* For the development of the analytical model for the prediction of a central value of NS pulse-like seismic demand (e.g. median of EDP given IM) and the associated dispersion around this central value, the methodology of [13] is followed. In this approach, the parameters of analytical functions are fitted against the 16%, 50% (median), and 84% fractile IDA curves of pulse-like FD ground motions. In the case of random variables following a normal distribution, which is a ubiquitous assumption in earthquake engineering for the logarithms of seismic demand quantities, the 16% and 84% fractiles correspond to the mean minus/plus one standard deviation interval boundaries, respectively.

In the literature, the question of which measure of central value (mean or median) is most convenient for the development of predictive equations for inelastic seismic demand will sporadically emerge (e.g. [29, 30]). For this particular case, the sample median is chosen because of its characteristic of robust estimator. The presence of a descending branch on the backbone of the oscillators examined, means that the model will have to tackle the issue of predicting the distribution of collapse capacity $R_{cap}$, defined as the intensity level which causes dynamic instability of the SDOF system. Yet with the appearance of collapse points on the individual IDA curves (Figure 4), the sample mean of EDP given IM (EDP|IM) can be no longer defined. On the other hand, the counted median is not subject to such restrictions [31]. Furthermore, it was shown in [12] that the x% fractile IDA curves of $EDP_{x\%}|IM$ and $(100-x\%)$ IDA fractiles of $IM_{(100-x)\%}|EDP$ are almost identical, with collapse capacity fractile points $R_{cap,(100-x)\%}$ belonging to both the $\mu_{x\%}|R$ and $R_{(100-x)\%}|\mu$ fractile IDA curves. It was observed during the present study that the same properties hold for pulse-IDAs. Therefore, the use of the three fractiles to capture central value and dispersion provides some flexibility, which in turn allows for the efficient modelling of seismic demand in terms of both EDP|IM and IM levels causing dynamic instability.

A final point to address regarding the statistical aspects of the model is that of preferring a triple curve-fitting operation of the three fractiles rather than regression analysis. Ordinary least-squares regression works under the typical assumption of Gaussian, independent and identically distributed (i.i.d.) residuals [32]. Although the Gaussian distribution of the residuals can sometimes be achieved by some transformation of the independent variable, meeting the i.i.d. conditions of an oscillator's responses across all IM levels is problematic. First of all, the variance of SDOF inelastic response is known to increase at higher IM levels [33] (identical distributions imply constant variance). Furthermore, the probabilistic distribution of the responses is disrupted when reduction factor tends to unity, or when very long period oscillators are considered, or when dynamic instability occurs. It is therefore unconvincing to make *a priori* assumptions on the probability distributions underlying the model for the purposes of regression analysis; it is preferable to simply fit parametric curves to their sample fractiles. Assumptions on the nature of these distributions can then be made in due time, as dictated by the necessities of eventual applications of the model (refer also to [17]).

*2.4.2. Predictor variables and explanatory value of the $T/T_p$ ratio.* An analytical model of seismic demand for SDOF oscillators featuring a generic trilinear backbone will necessarily include all the parameters that uniquely define the geometry of the backbone curve. Therefore, $\alpha_h$, $\mu_c$, and $\alpha_c$ (Figure 2) should be included as covariates in the model. The effect of varying these parameters on the seismic response to pulse-like ground motions has already been the object of previous investigation [34]. The additional variables that will be included in the model are pulse period, by virtue of its demonstrable value as a predictor of inelastic response for NS-FD ground motions that was confirmed numerous times in past studies [16, 25, 26] and the period of natural vibration T. In fact, these two variables are combined into the normalized period ratio $T/T_p$, in a manner analogous to [16, 17, 19]. The decision to base the model on the $T/T_p$ ratio was alluded to during the definition of pulse-IDA curves. Nevertheless, in a preliminary version of the model by the same authors [35], a concern had already been raised about mixing the response of very low period oscillators with that of long-period systems within a single $T/T_p$ cross section of data. In fact, in that work, it was suggested that at each $T/T_p$ ratio, responses from oscillators with natural period $T \leq 0.30s$ be omitted from the model. That decision was based on engineering judgement, which dictated that it is prudent to keep the responses of low-period oscillators, which are characterized by high ductility demands even when ordinary records are concerned, separated from the responses of moderate-to-long period oscillators subjected to long-duration pulses.

In the present study, the intention is to evaluate the explanatory value of the ratio $T/T_p$ with respect to NS pulse-like inelastic demand in a systematic way. More specifically, it will be examined whether or not there is a *statistically significant* effect of the period of natural vibration in the prediction of said inelastic response, which is captured in its entirety by the $T/T_p$ ratio. The methodology chosen for this investigation of the role of period T employs statistical hypothesis testing. The first step of this procedure is to obtain the sample of ductility demand responses of a specific SDOF system at a 'stripe' of given reduction factor R and $T/T_p$ ratio. These original samples of responses from 130 FD records are then divided into smaller subsets, each subset consisting of responses corresponding to oscillators with period T contained within a predefined interval $T_A < T \leq T_B$ (non-overlapping period intervals are always employed). The second step consists of comparing the central values of these new subsets among one another for systematic differences. Because of the dispersion of each stripe, a direct comparison between sample means or medians is not meaningful; instead, a statistical comparison must be performed by each time testing the *null hypothesis* (denoted $H_o$) that '*the two sets of responses have been sampled from normal distributions with equal medians (but possibly unequal variances)*'.

The practical end result of this procedure is to identify such boundaries $T_A$, $T_B$ as to observe systematic rejection of $H_o$ among the corresponding intervals, thus hinting at the need for separate analytical modelling of NS-FD seismic demand for each interval. Note, however, that because of the probabilistic nature of these tests it is possible to encounter some rejections even if $H_o$ holds true and vice-versa. In order to perform the test, one should define what can be considered as acceptable risk, $\alpha$, of rejecting the null hypothesis, when it is actually correct (which is also known in statistical literature as a type I error, [36]). This concept is represented as a conditional probability in Eqn 3. In this case, $\alpha = 0.05$ is considered.

$$\alpha = P[\text{reject } H_o | H_o \text{ correct}] \tag{3}$$

For the purposes of this investigation, $H_o$ was subjected to the Aspin–Welch test ([37]) for the cases of three bilinear oscillators with hardening stiffness ratios $\alpha_h = \{0.00, 0.10, 0.30\}$, five normalized period ratios $T/T_p = \{0.20, 0.30, 0.40, 0.80, 1.20\}$, three levels of strength reduction factor $R = \{2.4, 4.0, 5.5\}$, and a non-overlapping tri-interval partitioning of the period domain $T \leq T_A$, $T_A < T \leq T_B$ and $T > T_B$. Thus, each time the interval limits $T_A, T_B$ were shifted in order to explore the period domain for statistically significant differences in median ductility demand within a $T/T_p$ cross section, a maximum of 180 $t$-statistics and corresponding $p$-values were calculated (at times less as some combinations of $T/T_p$ and $T_A, T_B$ leave some stripes devoid of records).

Note that the analytical model for the bilinear hardening case also serves as a component of the complete trilinear model (both presented in the following). Therefore, examining bilinear hardening oscillators for eventual statistically significant effects of T will eventually reflect upon the entire model. Some characteristic results are given in Table I and a graphical representation in Figure 5.

The choice of test type can be explained by the fact that the two stripes to be compared each time contain responses from oscillators with different periods and thus heteroscedasticity (unequal variances) was assumed. Because of the assumption of sampling normally distributed populations, the test is performed on the logarithms of ductility demands of hardening bilinear systems for each pair of stripes. This is consistent with the methodology followed in [38] and [39] (in the latter case equal, yet unknown, variances were a more logical assumption leading to a simple $t$-test being adopted). The degrees of freedom of the distribution of the test statistic in the presence of the heteroscedasticity assumption were approximated according to [40].

Generally speaking, rejecting the null hypothesis or not was dominated by the ratio $T/T_p$ and the interval boundaries $T_A, T_B$. In other words, given $T/T_p, T_A, T_B$, the tendency to reject $H_o$ or not at $\alpha = 0.05$ was more or less uniform across the three bilinear oscillators and the three reduction factors considered. Most cases of statistically significant differences in the median ductility demands (i.e. cases when $H_o$ was rejected) were encountered for $T/T_p$ ratios between 0.20 and 0.40. These hypothesis tests emphatically confirmed the premise already made in [35], that NS seismic demand is systematically different for oscillators with $0.10s < T \leq 0.30s$ compared with that of SDOF systems with $T > 0.30s$. Less pronounced systematic differences were detected between low to moderate-period oscillators and long to very-long-period oscillators, when $T/T_p < 0.50$.

Another interesting observation is that when long period values were selected for $T_B$ and stripes at $T > T_B$ and $T/T_p = 1.20$ or higher were tested (corresponding to very-high-period systems), $H_o$ was consistently rejected across all parameters considered. In order to interpret this behaviour, one has to look at the entire logical complement of $H_o$ and deduce that rejection does not only come from existence of a statistically significant difference between the logarithmic means but it can also result from not sampling a Gaussian distribution. In fact, when very long period oscillators are considered, inelastic displacements tend to cluster around the peak ground displacement even at high levels of inelasticity (for an explanation of this phenomenon refer to Chopra and Chintanapakdee [41]) in a quasi-deterministic manner, thus departing from the empirical distributions encountered for lower period systems.

Because of the previously mentioned observations, it was decided to develop the analytical model by providing separate pulse-IDA curve fits for certain 'spectral regions' (i.e. period intervals) and $T/T_p$ ratios. Therefore, in what follows, parameter estimation for the analytical functions is always performed by fitting the model against the data for the following distinct cases:

- Systems with $0.10s < T \leq 0.30s$ when $0.10 \leq T/T_p \leq 0.30$.
- Systems with $0.30s < T \leq 0.80$ s when $0.10 \leq T/T_p \leq 0.50$.
- Systems with $T > 0.80s$ when $0.15 \leq T/T_p \leq 0.50$.
- Systems of all periods not falling into one of the previously mentioned categories are covered by a single model valid for $0.10 \leq T/T_p \leq 2.00$.

In overview of the salient points pertaining to the methodology adopted for this study, it can be said that IDA is performed for a population of moderately pinching SDOF systems with bilinear and trilinear backbones, using a suite of NS-FD ground motions. Median and 16%, 84% sample fractile IDA curves

Table I. Some illustrative test statistics (β denotes standard deviation of log-ductility) and rejection/non-rejection results for the null hypothesis that the pairs of ductility demand stripes have been sampled from normal distributions with equal medians but different variances.

| Sample characteristics | | $i$ | Sample size $N_i$ | sample stripe R factor | $\overline{\ln\mu_i}$ | $\beta_i$ | Test statistic | $\nu$ DoF | $p$-value | Reject/do not reject $H_o$ at $\alpha = 0.05$ |
|---|---|---|---|---|---|---|---|---|---|---|
| $\alpha_h = 0$ $\frac{T}{T_p} = 0.20$ | 0.10s < T ≤ 0.30s | 1 | 49 | R = 2.4 | 1.999 | 0.871 | 4.5477 | 80 | $1.9 \cdot 10^{-5}$ | Reject |
| | 0.30s < T ≤ 0.80s | 2 | 34 | | 1.280 | 0.568 | | | | |
| | 0.10s < T ≤ 0.30s | 1 | 49 | R = 4.0 | 3.117 | 0.888 | 5.2431 | 74 | $1.4 \cdot 10^{-6}$ | Reject |
| | 0.30s < T ≤ 0.80s | 2 | 34 | | 2.122 | 0.830 | | | | |
| | 0.10s < T ≤ 0.30s | 1 | 49 | R = 5.5 | 3.635 | 0.769 | 5.2734 | 66 | $1.6 \cdot 10^{-6}$ | Reject |
| | 0.30s < T ≤ 0.80s | 2 | 34 | | 2.677 | 0.843 | | | | |
| $\alpha_h = 0$ $\frac{T}{T_p} = 0.30$ | 0.30s < T ≤ 1.20s | 1 | 56 | R = 2.4 | 1.287 | 0.555 | 1.6147 | 100 | 0.1095 | Do not reject |
| | T > 1.20s | 2 | 47 | | 1.127 | 0.455 | | | | |
| | 0.30s < T ≤ 1.20s | 1 | 56 | R = 4.0 | 2.201 | 0.712 | 2.0804 | 100 | 0.0400 | Reject |
| | T > 1.20s | 2 | 47 | | 1.931 | 0.604 | | | | |
| | 0.30s < T ≤ 1.20s | 1 | 56 | R = 5.5 | 2.640 | 0.685 | 1.9209 | 99 | 0.0576 | Do not reject |
| | T > 1.20s | 2 | 47 | | 2.387 | 0.651 | | | | |
| $\alpha_h = 0.10$ $\frac{T}{T_p} = 0.40$ | 0.30s < T ≤ 0.80s | 1 | 50 | R = 2.4 | 1.284 | 0.413 | 1.9700 | 98 | 0.0516 | Do not reject |
| | T > 0.80s | 2 | 66 | | 1.138 | 0.368 | | | | |
| | 0.30s < T ≤ 0.80s | 1 | 50 | R = 4.0 | 2.110 | 0.475 | 3.1615 | 101 | 0.0021 | Reject |
| | T > 0.80s | 2 | 66 | | 1.836 | 0.443 | | | | |
| | 0.30s < T ≤ 0.80s | 1 | 50 | R = 5.5 | 2.530 | 0.476 | 3.4474 | 105 | 0.0008 | Reject |
| | T > 0.80s | 2 | 66 | | 2.223 | 0.472 | | | | |
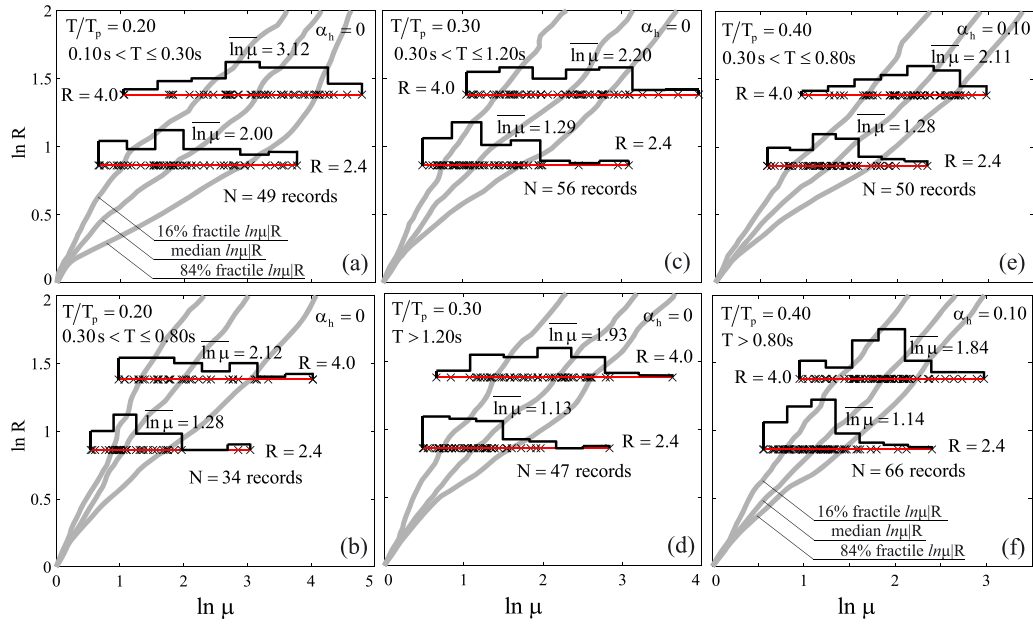
Figure 5. Graphical representation for some of the stripes of log-ductility demand given reduction factor, $T/T_p$ ratio and period range, whose means have been statistically tested for equality (detailed results of the corresponding tests are among those provided in Table I) . Stripes in panels (a) and (b) correspond to bilinear systems with $\alpha_h = 0$ (elastic-perfectly-plastic oscillators), which maintain a ratio of $T/T_p = 0.20$. Panel (a) refers to oscillators within the $0.10s < T \leq 0.30s$ interval, while panel (b) to those within $0.30s < T \leq 0.80s$. Samples between (a) and (b), at each level of reduction factor shown, have been used to test the null hypothesis $H_o$ at $\alpha = 0.05$. The same is true for the response samples between panels (c) and (d) ($\alpha_h = 0$, $T/T_p = 0.30$, test between $0.30s < T \leq 1.20s$ and $T > 1.20$ s intervals) as well as (e) and (f) ($\alpha_h = 0.10$, $T/T_p = 0.40$, test between $0.30s < T \leq 0.80s$ and $T > 0.80s$ intervals).

are obtained for each oscillator at various constant $T/T_p$ ratios and are subsequently modelled analytically by means of least-squares curve fitting. The model distinguishes between specific spectral regions in order to better capture the combined effect of $T$ and $T_p$ on NS pulse-like seismic demand. Details on the functional forms and the actual curve-fitting procedures are provided in the following sections.

## 3. BILINEAR HARDENING SDOF SYSTEMS

The analytical functional form selected to model the pulse-like IDA curves for bilinear oscillators with hardening behaviour (positive post-yield slope) is given by Eqn 4. It is a rational function (in log-space) of ductility given reduction factor fractiles, containing four parameters to be determined by fitting the model to the data. A total of four-hundred sets of IDA curves were obtained for this purpose, corresponding to combinations of post-yield stiffness ratios $\alpha_h$ spanning the interval $[0, 0.9]$ and $T/T_p$ ratios belonging within $[0.1, 2.0]$.

$$\ln\mu_{x\%} = \frac{a_{x\%} \cdot \ln^2 R + b_{x\%} \cdot \ln R}{c_{x\%} \cdot \ln R + d_{x\%}}, x = \{16, 50, 84\}, R \in [1, R_{(100-x)\%}(\mu_c)], \mu_c \in (1, 15),$$

$$a_{x\%}, b_{x\%}, c_{x\%}, d_{x\%} = g(\alpha_h, T/T_p, T), \alpha_h \in [0, 0.9], T/T_p \in [0.1, 2.0], T > 0.10s \qquad (4)$$

The term $R_{(100-x)\%}(\mu_c)$ appearing in the domain definition of reduction factor R in Eqn 4 is the reduction factor corresponding to the capping point of a trilinear backbone oscillator. The implication is that up to the point of capping ductility $\mu_c$, this equation is also valid for the general trilinear case (detailed treatment to follow).

The curve-fitting procedure entails obtaining non-linear least-squares estimates for the model parameters $a_{x\%}, b_{x\%}, c_{x\%}$ and $d_{x\%}$ for each distinct combination of $\alpha_h$, $T/T_p$ and each fractile $x\% = \{16\%, 50\%, 84\%\}$. As elaborated during the preceding discussion on methodology, these fractiles are also calculated among sub-sets of the employed record suite. This means that for $T/T_p \in [0.1, 0.3]$ the three fractiles are also calculated among the pulse-like records which correspond to oscillator periods within the interval $T \in (0.10s, 0.30s]$, and this is repeated for $T/T_p \in [0.1, 0.5]$, $T \in (0.30s, 0.80s]$ and for $T/T_p \in [0.15, 0.5]$, $T > 0.80s$. Thus, separate sets of parameters are derived for such period intervals (or spectral regions) as have been deemed statistically meaningful by prior analysis.

Overall, this curve-fitting procedure leads to groups of model parameters $a_{x\%}, b_{x\%}, c_{x\%}$ and $d_{x\%}$ that, given period T, are *implicit* functions of post-yield stiffness ratio $\alpha_h$ (which uniquely characterizes the shape of this type of backbone), normalized period $T/T_p$ and the $x\%$ fractile IDA of interest—hence the notation $g(\alpha_h, T/T_p, T)$ in Eqn 4. In a preliminary version of the model [17] and also in [13], a second stage of fitting was conducted, in order to render the model parameters *explicit* analytical functions of $\alpha_h$ and $T/T_p$ (in [17]) or T (in the case of ordinary records [13]). However, these past endeavors also showed that the dependence of the model parameters on $\alpha_h$ and $T/T_p$ or T is quite complex and can lead to very elaborate equations. These additional analytical functions have the advantage of lending elegance to the solution but also the disadvantages of lacking straightforward physical interpretation and adding a second source of misfit of the model to the data.

In the present study, it was decided to obtain results for a finer grid of $\alpha_h$, $T/T_p$ values and subsequently tabulate the single stage fit results in a manner that lends itself to linear interpolation. In fact, these results have been gathered into MATLAB® data structures and incorporated into MATLAB scripted functions that handle the necessary interpolations. These tools are available as electronic supplements to this paper [42]. In Figure 6, several examples of the fitted model against the original pulse-IDA fractile points are presented, highlighting the efficiency of the chosen functional form of Eqn 4 in capturing the shifting trends of the data among variations in spectral region, $T/T_p$ and $\alpha_h$.
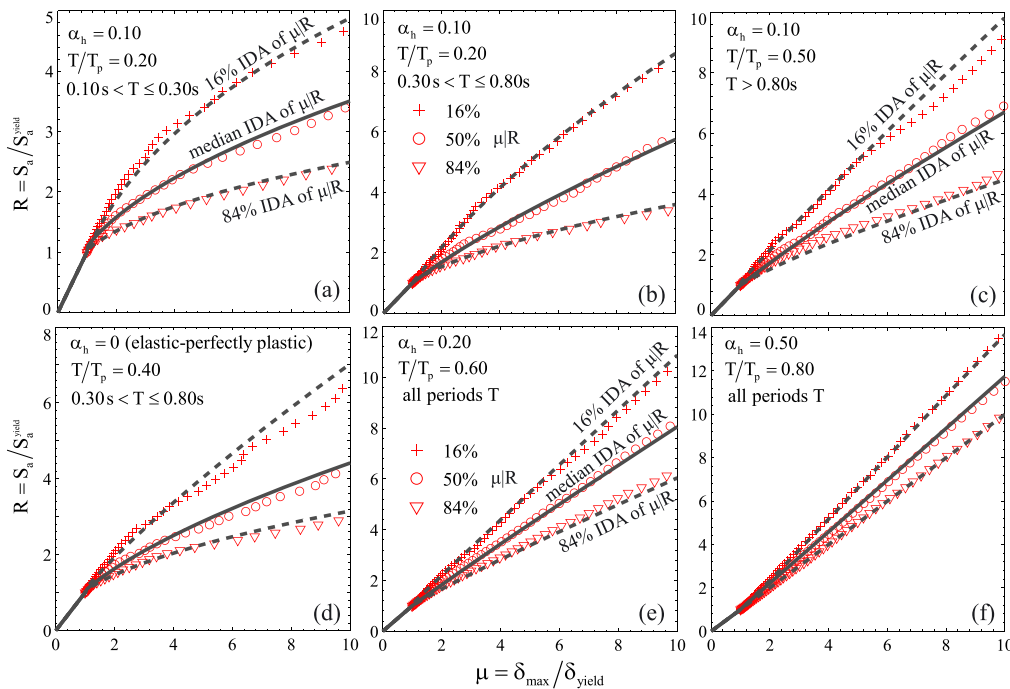


Figure 6. Comparison of the fitted model of Eqn 4 with the underlying data for SDOF systems (a) with $\alpha_h = 10\%$ at $T/T_p = 0.20$ when $0.10s < T \leq 0.30s$, (b) $\alpha_h = 10\%$ at $T/T_p = 0.20$ when $0.30s < T \leq 0.80s$, (c) $\alpha_h = 10\%$ at $T/T_p = 0.50$ when $T > 0.80s$, (d) $\alpha_h = 0$ at $T/T_p = 0.40$ when $0.30s < T \leq 0.80s$ ,(e) $\alpha_h = 20\%$ at $T/T_p = 0.60$ for all periods T, and (f) $\alpha_h = 50\%$ at $T/T_p = 0.80$ for all periods T.

### 4. NEGATIVE POST-YIELD STIFFNESS BILINEAR SDOF SYSTEMS

The model-fitting procedure in the case of bilinear SDOF oscillators with softening behaviour (negative post-yield stiffness ratio) is in principle similar to what has been already presented for the hardening case. The main difference stems from the fact that the appearance of a negative-stiffness branch on the backbone curve requires the introduction of collapse capacity fractiles $R_{cap,x\%}$ into the model (i.e. strength reduction factor that causes dynamic instability in x % of the ground motions, as defined previously). This important additional consideration, led to the adoption of the functional form of Eqn 5, which models reduction factor given ductility (fractile $R_{x\%}|\mu$), as opposed to the $\mu$ given R fractiles ($\mu_{x\%}|R$) of Eqn 4 fitted against the hardening cases. It is recalled that according to [24], the $\mu_{x\%}|R$ and $R_{x\%}|\mu$ fractile IDA curves are almost identical, even when the typical IDA properties of continuity and monotonicity are slightly violated. The reason for invoking this 'reversal' property is related to the analytical treatment implemented for the inclusion of collapse capacity $R_{cap}$ into the model and shall become apparent shortly.

$$\ln R_{x\%} = \frac{a_{x\%} \cdot \ln\mu}{\ln\mu + b_{x\%}}, \mu \in \left(1, \mu_{cap(100-x)\%}\right], x = \{16, 50, 84\},$$
$$a_{x\%}, b_{x\%} = g\left(|\alpha_c|, T/T_p, T\right), \alpha_c \in [-4.0, -0.01], T/T_p \in [0.1, 2.0], T > 0.10s \quad (5)$$

As in the hardening case, Eqn 5 represents a non-linear model with respect to its parameters $a_{x\%}$ and $b_{x\%}$. Weighted least-squares estimates are obtained by fitting the relevant fractiles (for the same period intervals as before) against six-hundred and twenty combinations of $T/T_p \in [0.1, 2.0]$ and post-cap stiffness ratio $\alpha_c \in [-4.0, -0.01]$. The fractile ductility $\mu_{cap(100-x)\%}$ appearing in Eqn 5 is the ductility at capacity (not to be confused with capping ductility $\mu_c$), that is ductility where dynamic instability occurs and therefore collapse capacity $R_{cap,x\%}$ is reached. While dynamic instability is strictly expected at the point of crossing the zero capacity axis at $\mu_{end}$ — Eqn 1 — issues of numerical accuracy may often cause its earlier appearance, thus necessitating the introduction of $\mu_{cap(100-x)\%}$ to reconcile the practical with the ideal. The weighting scheme implemented into the fitting procedure is intended to guarantee good local fit of Eqn 5 at the capacity point $\{\mu_{cap(100-x)\%}, R_{cap,x\%}\}$. Then, the fractiles of ductility at capacity are included into the model by also fitting Eqn 6 against the results of the same bilinear softening systems:

$$\mu_{cap,x\%} = \mu_c + c_{x\%} \cdot [1 + \alpha_h \cdot (\mu_c - 1)]/|\alpha_c|,$$
$$\alpha_h \in [0, 0.9), \alpha_c \in [-4.0, -0.05), x = \{16, 50, 84\} \quad (6)$$

The notation in Eqn 6 corresponds to the general trilinear case, and its purpose will be revealed in the following section. In fact, for a purely bilinear softening case, Eqn 6 reduces to $\mu_{cap,x\%} = 1 + c_{x\%}/|\alpha_c|$.

Recalling that the weighted least squares fitting of Eqn 5 practically forces it to pass through the capacity point, we can calculate an analytical prediction for capacity fractiles $R_{cap,x\%}$ by merely substituting the result of Eqn 6 into Eqn 5 and thus obtain

$$\ln R_{cap,x\%} = \frac{a_{x\%} \cdot \ln\mu_{cap(100-x)\%}}{\ln\mu_{cap(100-x)\%} + b_{x\%}}, x = \{16, 50, 84\} \quad (7)$$

Note that the domain of post-capping slope $\alpha_c$ for Eqn 5 is $[-4.0, -0.01]$, while that of Eqn 6 is $[-4.0, -0.05)$. The reason behind this is that systems with $0.01 \leq |\alpha_c| < 0.05$ will experience dynamic instability at very high ductility and may exhibit highly-irregular non-monotonic $R_{84\%}|\mu$ (or $\mu_{16\%}|R$) fractiles. In fact, it was deemed counter-productive to model this behaviour up to the point of collapse when said point corresponds to unrealistic ductility demands. Thus, oscillators with
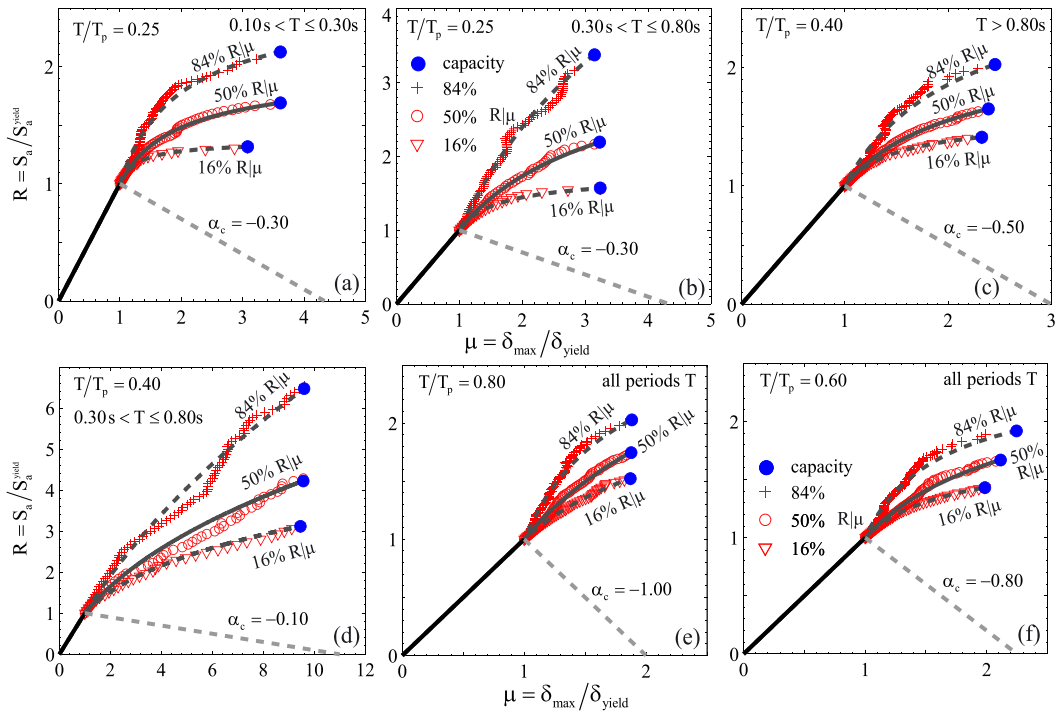
Figure 7. Comparison of the fitted model of Eqns 5–7 with the underlying data for bilinear softening systems with $\alpha_c = -30\%$ at $T/T_p = 0.25$ when (a) $0.10s < T \le 0.30s$ and when (b) $0.30s < T \le 0.80s$, (c) $\alpha_c = -50\%$ at $T/T_p = 0.40$ when $T > 0.80s$, (d) $\alpha_c = -10\%$ at $T/T_p = 0.40$ when $0.30s < T \le 0.80s$, (e) $\alpha_c = -100\%$ at $T/T_p = 0.80$ for all periods $T$, and (f) $\alpha_c = -80\%$ at $T/T_p = 0.60$ for all periods $T$.

a softening branch falling in the $0.01 \le |\alpha_c| < 0.05$ range were modelled via Eqn 5 up to a ductility of fifteen and were excluded from the $R_{cap,x\%}$ part of the model.

Similar to the hardening case, model parameters $a_{x\%}, b_{x\%}, c_{x\%}$ are treated as implicit functions of $\alpha_c, T/T_p$ for each period range and fractile $x\%$ and are available within a MATLAB function provided among the electronic supplements to this paper [42]. Figure 7 offers a representation of the curve-fitting results for bilinear softening SDOF systems, for a variety of cases. An interesting observation stemming from the figure is that, because Eqn 5 tends towards flatter slopes near the capacity point, eventual misfit of the model in terms of $\mu_{cap,x\%}$ will produce a much lesser variation in $R_{cap,(100-x)\%}$. This is advantageous, because the latter is the more important statistic.

## 5. MODEL FOR THE COMPLETE TRILINEAR BACKBONE

### 5.1. Equivalent ductility concept

A straightforward, if somewhat impractical, way of tackling the problem of modelling pulse-like IDAs for systems boasting a complete trilinear backbone could be to simply run a large number of analyses in an attempt to span the entire parameter space of $\{\alpha_h, \mu_c, \alpha_c, T, T_p\}$, as was performed for the two bilinear cases already covered. However, structural responses exhibit a complicated interdependency with respect to these five parameters, which cannot be studied independently one from another. Actually, considering all their meaningful combinations in an attempt to attain the same refinement as before would require an estimated one-hundred and twenty thousand IDA sets.

Instead, the methodology developed in [13] can also be adapted to the pulse-like case, drastically reducing the amount of necessary analyses. More specifically, it was found that the equivalent ductility concept (Figure 8), which was introduced in the analogous study of ordinary ground motion SDOF IDAs, could also be employed for the case at hand. In that study it was found that a
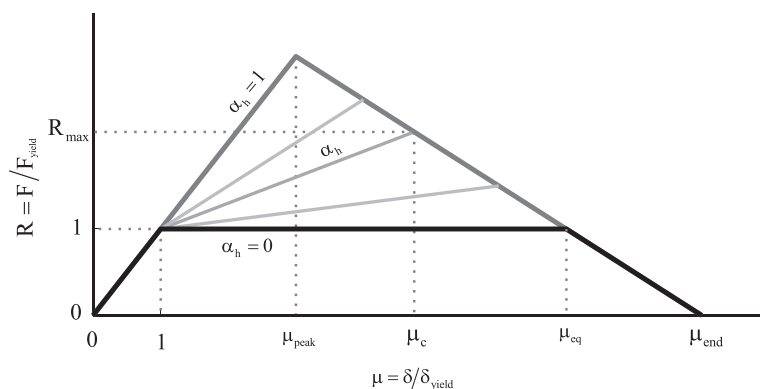
Figure 8. Illustration of a set of backbones belonging to the same family and auxiliary parameters pertaining to the equivalent ductility concept

'family' of oscillators with a generic backbone containing both hardening segments and negative-stiffness softening branches with coincident post-capping slope, such as those shown in Figure 8, have a very similar part of the IDA fractile curves between capping ductility and the point of collapse capacity. Furthermore, collapse capacity $R_{cap}$ (or 'flat-line height' if one were to adopt the terminology introduced in [12]) among these oscillators varies in an almost linear fashion between two bounding values, defined by the responses of the $\alpha_h = 1$ and the $\alpha_h = 0$ backbones of the 'common post-capping-segment family'.

Thus, for any trilinear oscillator with given hardening slope $\alpha_h$, capping ductility $\mu_c$, and post-capping slope $\alpha_c$, one initially needs to determine the defining parameters of these two auxiliary limit cases in the backbone family, that is peak ductility $\mu_{peak}$ and equivalent ductility $\mu_{eq}$:

$$\mu_{peak} = [1 + \mu_c \cdot |\alpha_c| + \alpha_h \cdot (\mu_c - 1)]/(1 + |\alpha_c|) \tag{8}$$

$$\mu_{eq} = \mu_c + \alpha_h \cdot (\mu_c - 1)/|\alpha_c| \tag{9}$$

Since the first auxiliary backbone is nothing more than a bilinear-softening case scaled by a factor of $\mu_{peak}$ and has therefore already been covered by the analytical model, all that is missing are the collapse capacity fractiles $R_{cap,x\%}$ of the 'equivalent ductility' oscillator with $\alpha_h = 0$ and $\mu_c = \mu_{eq}$.

### 5.2. Complete model for trilinear backbone SDOF oscillators

For a given generic trilinear backbone, it is trivial that up to capping ductility $\mu_c$ all individual pulse-IDAs coincide with those of a bilinear system with the same $\alpha_h$, and therefore, the same is true for the fractiles. Therefore, Eqn 4 can be used to analytically model this segment. The remaining part of the fractile pulse IDAs for the trilinear backbone corresponds to an $\mu_{peak}$—times scaled version of the corresponding bilinear softening system, adjusted vertically to produce the $\widehat{R}_{x\%}(\mu_c)$, which is the capacity obtained by substituting $\mu_{(100-x)\%} = \mu_c$ in Eqn 4, in order to ensure continuity:

$$R_{x\%} = R^o_{x\%}(\mu_c) + \mu_{peak} \cdot \exp\left(\frac{a_{x\%} \cdot \ln\mu}{\ln\mu + b_{x\%}}\right), \mu \in \left(\mu_c, \mu_{cap(100-x)\%}\right], x = \{16, 50, 84\} \tag{10}$$

$$R^o_{x\%}(\mu_c) = \widehat{R}_{x\%}(\mu_c) - \mu_{peak} \cdot \exp\left(\frac{a_{x\%} \cdot \ln\mu_c}{\ln\mu_c + b_{x\%}}\right), x = \{16, 50, 84\} \tag{11}$$

Finally, an adjustment is applied to the collapse capacity to account for the fact that the generic trilinear oscillator is observed to exhibit dynamic instability at reduction factors progressively

greater than the $\mu_{peak}$ softening bilinear model, with the largest adjustment corresponding to the equivalent ductility system. In order to model this effect, the collapse capacities for various trilinear backbones with $\alpha_h=0$ (e.g. Figure 9a) were obtained and a correction factor $d_{x\%}$ was fit against these results, leading to Eqn 12.

$$R_{cap,x\%} = \left(1 + d_{x\%} \cdot \frac{\mu_c - 1}{\mu_{eq} - 1}\right) \cdot \left[R_{x\%}^o(\mu_c) + \mu_{peak} \cdot \exp\left(\frac{a_{x\%} \cdot \ln\mu_{cap(100-x)\%}}{\ln\mu_{cap(100-x)\%} + b_{x\%}}\right)\right], x = \{16, 50, 84\},$$

$$d_{x\%} = g\left(\mu_{eq}, |\alpha_c|, T/T_p, T\right), \alpha_c \in [-4.0, -0.05], T/T_p \in [0.1, 2.0], T > 0.10s \qquad (12)$$

A comparison between the analytical predictions of the model and the calculated fractile pulse-IDAs for some trilinear backbones are shown in Figure 9. It is worth noting that the numerical results plotted in that figure against the analytical curves were not directly used to fit the model and were only obtained for the sake of evaluating the model's effectiveness.

## 6. DISCUSSION AND PROSPECTIVE APPLICATIONS

One of the most relevant evaluations that can be extracted from the analytical model presented in this paper is a direct comparison with the case of ordinary (i.e. non-impulsive) ground motions. To this end, the predictions of the SPO2IDA tool [14] were selected as representative of ordinary seismic demand at the SDOF level. Figure 10 presents some comparisons between median ordinary IDAs for a bilinear oscillator with $\alpha_h=20\%$, as provided by SPO2IDA, and the corresponding predictions of the NS pulse-like demand model proposed herein. The comparisons include several $T/T_p$ ratios and span all three 'spectral regions' of the proposed model.

At first glance, the comparison of pulse-like and ordinary median IDA curves makes it abundantly clear that the ratios of $T/T_p \leq 0.50$ contain pulse-like ground motions which are, in terms of median response, more aggressive than ordinary records. This comes as no surprise, as it only confirms what has been known from previous investigations [16, 25, 43]. However, the relative paucity of records that characterized earlier research on pulse-like seismic demand did not permit to fully appreciate if oscillators of various vibration periods behave in potentially different manner under these $T/T_p$ conditions.

In fact, it can be seen that low $T/T_p$ ratios of around 0.20 are particularly aggressive towards low-period oscillators, whereas for a ratio of around 0.60 the response is already slightly more benign than the ordinary case. On the other hand, for medium-period systems it is a $T/T_p$ of around 0.40
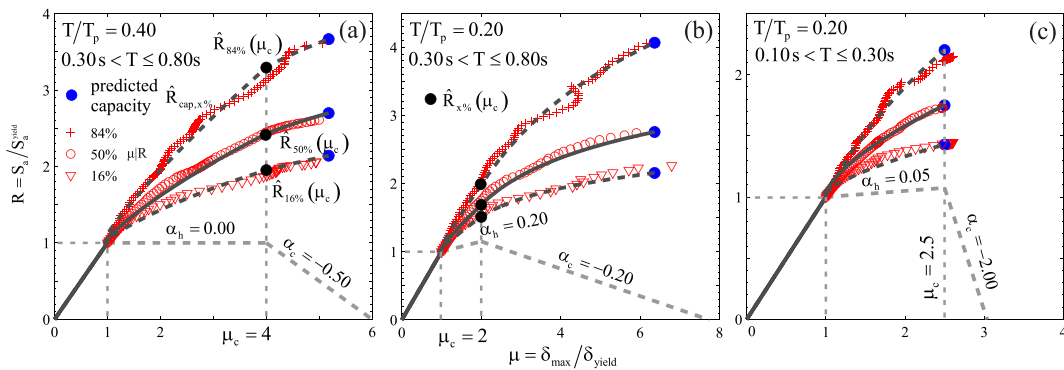


Figure 9. Comparison of the complete trilinear model prediction with corresponding numerical results for systems with (a) $\alpha_h=0$, $\mu_c=4$ and $\alpha_c=-50\%$ at $T/T_p=0.40$ when $0.30s < T \leq 0.80s$, (b) $\alpha_h=20\%$, $\mu_c=2$ and $\alpha_c=-20\%$ at $T/T_p=0.20$ for $0.30s < T \leq 0.80s$, and (c) $\alpha_h=5\%$, $\mu_c=2.5$ and $\alpha_c=-200\%$ at $T/T_p=0.20$ when $0.10s < T \leq 0.30s$.
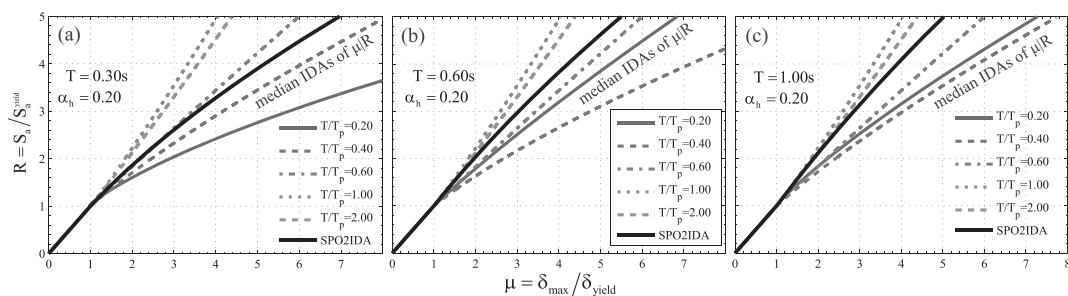
Figure 10. Comparisons between ordinary ground motion median IDA predictions (by SPO2IDA [13, 14]) for a bilinear SDOF system with $\alpha_h = 20\%$ and median IDA predictions for NS pulse-like ground motions for the same system and various $T/T_p$ ratios, according to the model presented in this study. The comparison is made for three periods of vibration, (a) $T = 0.30s$, (b) $T = 0.60s$, and (c) $T = 1.00s$, corresponding to all spectral regions of the pulse-IDA model.

that creates the highest median impulsive NS demand with the entire range of $T/T_p \leq 0.60$ still being on the aggressive side with respect to ordinary demand. For medium- to long-period oscillators, the most demanding pulses still appear to be centred around $T/T_p = 0.40$ with the region around 0.20 in close pursuit. For all spectral regions, it can be seen that in cases where the vibration period becomes comparable to or longer than the pulse duration, benign responses are to be expected on average. This is less pronounced in the medium- to long- period range, where response for $1.00 \leq T/T_p \leq 2.00$ and low reduction factors is comparable to ordinary demand. This last observation is also in agreement with previous research, since in [16] it was found that for $T/T_p > 0.80$ mean inelastic displacement ratios fall below unity.

Extending the comparison between pulse-like and ordinary ground motion-based models to trilinear SDOF systems with descending branches, one can also consider differences in predicted collapse capacity. In this case, it was observed that for systems with moderate-to-large ductility reserves, the same trends hold as seen in the preceding texts for bilinear hardening oscillators: pulse-like records appear more aggressive on average (lower collapse capacity) than ordinary ones for $T/T_p$ ratios lower than 0.60–0.75, with the lower bound corresponding to the low-period range and the upper to the longer periods. This can be seen in Figure 11(a–c), where median collapse capacity, for a moderately ductile system (capping ductility $\mu_c = 4$), as predicted by Eqn 12 is plotted as a function of $T/T_p$ and the SPO2IDA (ordinary) median prediction is denoted by a dashed horizontal line.

However, this trend does not hold for low-ductility, brittle systems, as can be seen in the second row of panels in Figure 11(d–f). In fact, for medium- to long-period systems with limited ductility reserves (e.g. the oscillator with capping ductility $\mu_c = 1.5$ used in Figure 11) the aggressive/benign threshold appears to move on to larger $T/T_p$ ratios with increasing period. For brittle systems at the longer-period 'spectral region', the same trend continues to a point where most $T/T_p$ ratios considered in the present model result in lower collapse capacities than ordinary records—on average. Furthermore, it can be seen that $T/T_p$ ratios around 0.50 tend to consistently exhibit the lowest $R_{cap,50\%}$ among impulsive records. Finally, it can be observed that past a certain $T/T_p$ ratio, whose value also varies according to available ductility, median collapse capacity remains relatively stable.

These observations are generally consistent with the findings of past research on collapse capacity of multiple degree of freedom systems subject to NS pulse-like motions [44, 45]. In [44] the transition $T/T_p$ ratio that sees stabilization of pulse-like collapse capacity was investigated against 10 building structures. A linear regression relation was established between available ductility of the structure and this transition ratio, which is found in good agreement with the predictions of Eqn 12. A similar trend was encountered in [45], where moving average curves of collapse capacity as functions of $T_p/T$ were calculated for 23 concrete frames. In that work, it was further observed that for some ductile multiple degree of freedom systems, pulse-like records with $T/T_p > 1.0$ can also be, on average, more aggressive than ordinary records. This effect can be attributed to excitation of the higher modes by the shorter pulse periods ([43, 45]), which cannot be captured by the SDOF model.
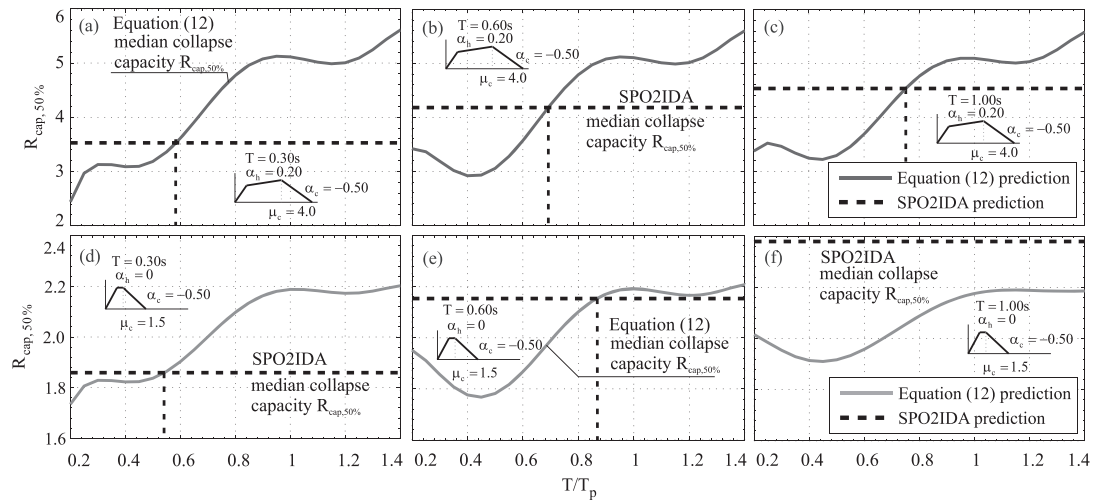
Figure 11. Comparison between median collapse capacity $R_{cap,50\%}$ predicted by Eqn 12 for pulse-like excitation at various $T/T_p$ ratios and SPO2IDA prediction for ordinary ground motions. The first row of panels refers to the trilinear backbone of a moderately ductile system ($\alpha_h = 0.20, \mu_c = 4.0, \alpha_c = -0.50$) with periods of vibration: (a) T = 0.30s, (b) T = 0.60s and (c) T = 1.00s. The second row corresponds to the trilinear backbone of a brittle system ($\alpha_h = 0, \mu_c = 1.50, \alpha_c = -0.50$) with periods of vibration: (d) T = 0.30s, (e) T = 0.60s, and (f) T = 1.00s.

Past investigations, where NS probabilistic seismic hazard analysis was implemented [22, 23], showcased the fact that a NS design scenario will not be necessarily restricted to a single $T_p$ dominating NS structural response (elastic and inelastic). In fact, it was found in certain case-studies that not only are different source to site configurations associated with different probability distributions of causal $T_p$ but that this is also true for a given site when increasing levels of seismic intensity are considered [8, 35] . It was also observed in those studies that at increasing IM levels, NS-FD can become increasingly important for the determination of site-specific mean inelastic demand. Be that as it may, it has been shown that as long as disaggregation of NS hazard can provide the necessary information on the probabilistic distribution of $T_p$ conditional on the design scenario of interest, analytical models containing pulse period as a predictor variable can be employed to estimate NS seismic demand or assess performance-based objectives under NS conditions. This was demonstrated in [8] for the case of single-stripe pushover-based simplified analysis using an earlier equation for NS-FD inelastic spectra [16]. More pertinent to the present model is the illustrative example included in [35], where a methodology for probabilistically incorporating $T_p$ into the calculation of NS inelastic demand at increasing levels of seismic intensity was demonstrated for a simple bilinear system. Extending that methodology into the realm of more complex multi-linear backbones is a necessary next step that will permit the application of the model presented in this study towards performance-based assessments in NS conditions.

## 7. CONCLUSIONS

The present study saw the use of IDA to investigate and model analytically the response of oscillators with trilinear backbone curves to near-source (NS) pulse-like ground motions. The proposed model uses equations to capture efficiently both median pulse-like demand and the associated heterogeneity. The analytical equations include pulse period as a predictor variable in the form of $T/T_p$ ratio but are also based on an extensive investigation that makes use of statistical inference to evaluate the simultaneous effect of vibration period within each $T/T_p$ bin. In order to describe mathematically the full range of response for the generic moderately pinching SDOF system subjected to pulse excitations, while keeping the computational load within manageable levels, the model is based on two primary components. Bilinear systems with either hardening or softening post-yield behaviour are investigated at length and non-linear least-squares curve fitting is employed to

simulate the corresponding pulse-IDA fractile curves. Subsequently, empirical rules and observations stemming from past research are exploited in order to assemble these results into a compact predictive model for the demand and capacity of the complete trilinear case, without having to resort to voluminous computations. The end-result constitutes an effective $R - \mu - T - T_p$ relation, which is provided to potential users in the form of MATLAB® code. Such a relation can draw upon the results of NS seismic hazard calculations in order to provide estimates of NS seismic demand that take FD effects into account in a consistent quantitative manner within the performance-based earthquake engineering framework.

## REFERENCES

1. Krawinkler H, Miranda E. Performance-based earthquake engineering. In: *Earthquake Engineering: From Engineering Seismology to Performance-Based Engineering*, Bozorgnia Y, Bertero VV (eds). CRC Press: FL, 2004.
2. Singh PJ. Earthquake ground motions: implications for designing structures and reconciling structural damage. *Earthquake Spectra* 1985; **1**(2):239–270.
3. Somerville PG, Smith NF, Graves RW, Abrahamson NA. Modification of empirical strong ground motion attenuation relations to include the amplitude and duration effects of rupture directivity. *Seismological Research Letters* 1997; **68**:199–222.
4. Baker JW. Quantitative classification of near-fault ground motions using wavelet analysis. *Bulletin of the Seismological Society of America* 2007; **97**(5):1486–1501.
5. Kalkan E, Kunnath SK. Assessment of current nonlinear static procedures for seismic evaluation of buildings. *Engineering Structures* 2007; **29**:305–316.
6. Fragiadakis M, Vamvatsikos D, Ascheim M. Application of nonlinear static procedures for seismic assessment of regular RC moment frame buildings. *Earthquake Spectra* 2014; **30**(2):767–794.
7. Fajfar P. Capacity spectrum method based on inelastic demand spectra. *Earthquake Engineering and Structural Dynamics* 1999; **28**:979–993.
8. Baltzopoulos G, Chioccarelli C, Iervolino I. The displacement coefficient method in near-source conditions. *Earthquake Engineering and Structural Dynamics* 2015; **44**(7):1015–1033.
9. Lignos D, Krawinkler H. Sidesway collapse of deteriorating structural systems under seismic excitations. Report No.177, The John A. Blume Earthquake Engineering Center, Stanford University, Stanford CA, 2012.
10. Liel AB, Haselton CB, Deirlein GG. Seismic collapse safety of reinforced concrete buildings. II: comparative assessment of nonductile and ductile moment frames. *Journal of Structural Engineering* 2011; **137**(4):492–502.
11. Adam C, Clemens J. Seismic collapse capacity of basic inelastic structures vulnerable to the P-delta effect. *Earthquake Engineering and Structural Dynamics* 2012; **41**:775–793.
12. Vamvatsikos D, Cornell CA. Incremental dynamic analysis. *Earthquake Engineering and Structural Dynamics* 2002; **31**:491–514.
13. Vamvatsikos D, Cornell CA. Direct estimation of the seismic demand and capacity of oscillators with multi-linear static pushovers through IDA. *Earthquake Engineering and Structural Dynamics* 2006; **35**:1097–1117.
14. SPO2IDA algorithm Excel® spreadsheet and MATLAB® implementations available online at: http://users.ntua.gr/divamva/software/spo2ida-allt.xls, http://users.ntua.gr/divamva/software/spo2ida-allt.zip
15. Shahi SK, Baker JW. An efficient algorithm to identify strong velocity pulses in multi-component ground motions. *Bulletin of the Seismological Society of America* 2014; **104**(5):2456–2466.
16. Iervolino I, Chioccarelli C, Baltzopoulos G. Inelastic displacement ratio of near-source pulse-like ground motions. *Earthquake Engineering and Structural Dynamics* 2012; **41**:2351–2357.
17. Baltzopoulos G, Structural performance evaluation in near-source conditions, PhD Thesis: Advisor I. Iervolino, Doctorate programme in Seismic Risk, XXVII cycle, Università degli Studi di Napoli Federico II, Naples, Italy, 2015. http://wpage.unina.it/iuniervo/doc_en/Students.html
18. Bray JD, Rodriguez-Marek A. Characterization of forward directivity ground motions in the near-fault region. *Soil Dynamics and Earthquake Engineering* 2004; **24**(11):815–828.
19. Ruiz-Garcìa J. Inelastic displacement ratios for seismic assessment of structures subjected to forward-directivity near-fault ground motions. *Journal of Earthquake Engineering* 2011; **15**(3):449–468.
20. Makris N, Black CJ. Dimensional analysis of bilinear oscillators under pulse-type excitations. *Journal of Engineering Mechanics* 2004; **130**(9):1019–1031.
21. Miranda E. Site-dependent strength reduction factors. *Journal of Structural Engineering* 1993; **119**(12):3503–3519.

22. Tothong P, Cornell CA, Baker JW. Explicit directivity-pulse inclusion in probabilistic seismic hazard analysis. *Earthquake Spectra* 2007; **23**:867–891.
23. Chioccarelli E, Iervolino I. Near-source seismic hazard and design scenarios. *Earthquake Engineering and Structural Dynamics* 2013; **42**:603–622.
24. Vamvatsikos D, Cornell CA. Applied incremental dynamic analysis. *Earthquake Spectra* 2004; **20**(2):523–553.
25. Akkar S, Yazgan U, Gülkan P. Deformation limits for simple non-degrading systems subjected to near-fault ground motions. Proceedings, 13th World Conference on Earthquake Engineering, Vancouver BC, Canada, Paper no. 2276, 2004.
26. Alavi B, Krawinkler H. Behavior of moment-resisting frame structures subjected to near-fault ground motions. *Earthquake Engineering and Structural Dynamics* 2004; **33**(6):687–706.
27. Ibarra LF, Krawinkler H. Global collapse of frame structures under seismic excitations. Report No.152, The John A. Blume Earthquake Engineering Center, Stanford University, Stanford CA, 2005.
28. Rahnama M, Krawinkler H. Effects of soft soils and hysteresis model on seismic demands. Report No. 108, The John A. Blume Earthquake Engineering Center, Stanford University, Stanford CA, 1993.
29. Dolsek M, Fajfar P. Inelastic spectra for infilled concrete frames. *Earthquake Engineering and Structural Dynamics* 2004; **33**:1395–1416.
30. Miranda E. Inelastic displacement ratios for structures on firm sites. *Journal of Structural Engineering* 2000; **126**(10): 1150–1159.
31. Shome N, Cornell CA. Probabilistic seismic demand analysis of nonlinear structures. RMS Report-35. Reliability of Marine Structures Group, Stanford University, Stanford CA, 1999.
32. Bates DM, Watt DG. Nonlinear regression analysis and its applications. John Wiley & Sons Inc,: New York, 1988.
33. Miranda E. Evaluation of site-dependent inelastic seismic design spectra. *Journal of Structural Engineering* 1993; **119**(5):1319–1338.
34. Dimakopoulou V, Fragiadakis M, Spyrakos C. Influence of modeling parameters on the response of degrading systems to near-field ground motions. *Engineering Structures* 2013; **53**:10–24.
35. Baltzopoulos G, Vamvatsikos D, Iervolino I. Near-source pulse-like seismic demand for multi-linear backbone oscillators. COMPDYN 2015, 5th ECCOMAS Thematic Conference on Computational Methods in Structural Dynamics and Earthquake Engineering, M. Papadrakakis, V. Papadopoulos, V. Plevris (eds.) Crete Island, Greece, 25–27 May 2015.
36. Mood AM, Graybill FA, Boes DC. *Introduction to the Theory of Statistics*. Mc-Graw Hill: New York, 1974.
37. Welch BL. The significance of the difference between two means when the population variances are unequal. *Biometrika* 1938; **29**:350–362.
38. Iervolino I, De Luca F, Cosenza E. Spectral shape-based assessment of SDOF nonlinear response to real, adjusted and artificial accelerograms. *Engineering Structures* 2010; **32**(9):2776–2792.
39. Iervolino I, Cornell CA. Record selection for nonlinear seismic analysis of structures. *Earthquake Spectra* 2005; **21**(3):685–713.
40. Shatterthwaite FE. Synthesis of variance. *Psychometrica* 1941; **6**(5):309–316.
41. Chopra A, Chintanapakdee C. Inelastic deformation ratios for design and evaluation of structures: single-degree-of-freedom bilinear systems. *Journal of Structural Engineering* 2004; **130**(9):1309–1319.
42. Electronic supplement to *Analytical modelling of near-source pulse-like seismic demand for multi-linear backbone oscillators* available online at: http://wpage.unina.it/iuniervo/PulseIDAs_matlab_scripts.rar
43. Tothong P, Cornell CA. Structural performance assessment under near-source pulse-like ground motions using advanced ground motion intensity measures. *Earthquake Engineering and Structural Dynamics* 2008; **37**(7):1013–1037.
44. Song S, Heaton TH. Predicting collapse of steel and reinforced-concrete frame buildings in different types of ground motions. *Proceedings of the 15th World Conference on Earthquake Engineering*, Lisbon, Portugal, 2012.
45. Champion C, Liel A. The effect of near-fault directivity on building seismic collapse risk. *Earthquake Engineering and Structural Dynamics* 2012; **41**:1391–1409.